Journal of Innovative Optical Health Sciences
Vol. 7, No. 1 (2014) 1350052 (7 pages)

DOI: 10.1142/S1793545813500521

World Scientific
www.worldscientific.com



# AUTOMATED ASSESSMENT OF EPIDERMAL THICKNESS AND VASCULAR DENSITY OF PORT WINE STAINS OCT IMAGE

CHENGMING WANG*, TIANCHENG HUO*, JING-GAO ZHENG*, NING ZHANG*, TIANYUAN CHEN*, WENCHAO LIAO*, YING WANG†, YING GU† and PING XUE*,‡

*Department of Physics and State Key Laboratory of Low-dimensional Quantum Physics
Tsinghua University, Beijing
100084, P. R. China

†Department of Laser Medicine
Chinese PLA General Hospital, Beijing
100853, P. R. China
‡xuep@tsinghua.edu.cn

Received 1 June 2013
Accepted 12 September 2013
Published 31 October 2013

Optical coherence tomography (OCT) enables *in vivo* imaging of port wine stains (PWS) lesions. The knowledge of vascular structure and epidermal thickness (ET) of PWS may aid the objective diagnosis and optimal treatment. To obtain the structural parameters more rapidly and avoid user intervention, an automated algorithm of energy map is introduced based on intensity and edge information to extract the skin surface using dynamic programming method. Subsequently, an averaged A-scan analysis is performed to obtain the mean ET and the relative intensity of dermis indicating the corresponding vascular density. This approach is currently successfully applied in clinical diagnosis and shows promising guidance and assessment of PDT treatment.

*Keywords*: Optical coherence tomography; port wine stains; epidermal thickness; image processing; photodynamic therapy.

## 1. Introduction

Port wine stains (PWS) is a common skin disease resulting from capillary dilation and malformation in the upper dermis of skin. Photodynamic therapy (PDT) has been widely used to treat PWS,[1] as it has a strongly selective effect on blood vessels. Injected with photosensitizer, patients are exposed to laser radiation. The photosensitizer generates singlet oxygen, which has an occlusion effect on microvessels. However, lacking of objective

diagnosis, the drug dose and laser parameters rely heavily on the skills of the doctors and their clinical experience.

Optical coherence tomography (OCT) is a non-invasive *in vivo* biomedical imaging modality. OCT stands out amongst other imaging techniques, with its high resolution and fast imaging speed, providing depth-resolved images. OCT is now being increasingly employed in dermatology.[2] Previous studies have shown that the mean epidermal thickness (ET) obtained by OCT can be considered as a quantitative parameter for skin diagnosis[3] and quantitative treatment effect assessment.[4,5] ET is also a good indicator of skin aging process.[6] ET correlates with laser dosage in PDT treatment, due to the epidermal absorption and scattering of light.[7] In our previous work,[8–10] manual line drawing method was used to measure ET in PWS OCT image. To obtain ET more rapidly and avoid user intervention, an automated algorithm is needed. In recent years, several automated methods have been reported to assess the ET by OCT, such as A-scan analysis,[3] shapelet analysis,[11] Markov chain[12] and active contour.[13] However, it is still unknown, about the effectiveness of these algorithms when applied to clinical OCT images with artifacts or skin/hair debris. In this paper, we propose and demonstrate an algorithm based on energy map that can assess the mean ET correctly and effectively even under the above condition.

In our previous work,[10] we demonstrated the blood vessel diameters measured manually in PWS OCT image which aids the objective diagnosis of PWS pathological types. However, automated extraction of these diameters was complicated and difficult, due to the irregular shape and nonclosure contour of capillary vessels. Therefore, in this paper, relative intensity of dermis is instead calculated to indicate the vascular structural parameters. This value can be achieved automatically in real time and shows statistical difference between PWS and contralateral normal skin.

## 2. Materials and Methods

### 2.1. *Handheld OCT system*

We used a handheld OCT system which had been described in detail elsewhere.[8] In brief, the system uses a light source with a center wavelength of 1310 nm, −3 dB bandwidth of 90 nm and an optical power of 9 mW. The system has a lateral resolution of 8 $\mu$m and an axial resolution of 7.4 $\mu$m, assuming that the mean skin index of refraction is 1.36.[14] Each B-scan consists of 400 × 400 pixels. The scanning range is 2.8 × 2.5 mm (axial × lateral).

### 2.2. *Clinical diagnosis of PWS*

A total of 51 Chinese patients, aged from 1 to 43 years, with PWS on the face and neck were recruited from outpatients of Department of Laser Medicine, Chinese PLA General Hospital. About 108 OCT images of PWS lesions and contralateral normal skin were obtained. Among the entire 108 images, the mean ET of 83 images could be measured manually using line drawing method by an experienced operator. These images are subsequently used for testing performance of the proposed algorithm.

### 2.3. *Skin surface detection*

The first procedure in our algorithm is to detect the air-skin surface. The surface contour is of great importance since it is severed as reference datum of measurements of ET measurements. It is not easy to determine the skin surface using simplified method. Severe artifacts such as saturation or shadowing would lead to invalidation of thresholding. In some images, the intensity of the dermo-epidermal junction is higher than that of the epidermis surface which may cause the failure of averaged A-scan method. Hair or skin flake near the surface may lead to error recognition. Therefore, we use a regularized shortest path[15] to obtain the exact surface boundary.

Figure 1 illustrates the pre-processing step. The depth of the maximum intensity of the averaged A-scans, named $d_{\max}$, is first identified. Subsequently, the region of interest (ROI) is set to the area whose depth range from $d_{\max} - 30$ pixels to $d_{\max} + 40$ pixels, as is displayed in Fig. 1(b). The ROI is chosen to include the complete air-skin surface while as small as possible to reduce the time consumption. In addition, the bottom area of 400 × 20 pixels of the image is considered as the background area.

The second step is the creation of an energy map or energy image. The energy map is of the same size of ROI, and each point of the map represents an

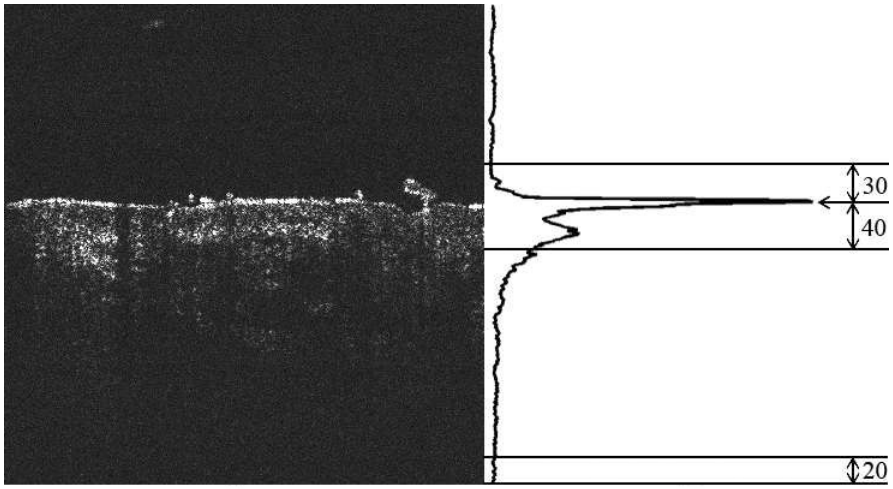


Fig. 1. Pre-processing step. (a) raw image. (b) ROI and background area.

energy. We define the energy map $E$ as below.

$$E(n_j, j) = -[\lambda_1 I_s(n_j, j) + \lambda_2 I_c(n_j, j) + \lambda_3 I_i(n_j, j)], \quad (1)$$

where $n_j$ and $j$ denote the row and column of $E$, respectively. $I_i$ is the image intensity map by intensity detector, $I_s$ is horizontal edges map by Sobel edge-detector, $I_c$ is horizontal and vertical edges map by Canny edge-detector, and $\lambda_1, \lambda_2, \lambda_3$ are the weighted factors. Figures 2(a)–2(d) show the raw ROI and $I_i$, $I_c$, $I_c$, respectively. Figure 2(e) illustrates the weighted sum of Figs. 2(b)–2(d) and its high intensity indicates high possibility of skin surface. The energy is designed to be negative facilitating substantive shortest path.

The third step is to solve the shortest path of energy $E$ by the use of regularized dynamic programming. A path $P$ of $p$th order connectivity that crosses the energy map from the left side to the right side is given by:

$$P = \{(n_1, 1), \ldots, (n_j, j), \ldots (n_{400})\}, \quad |n_{j+1} - n_j| \leq p. \quad (2)$$

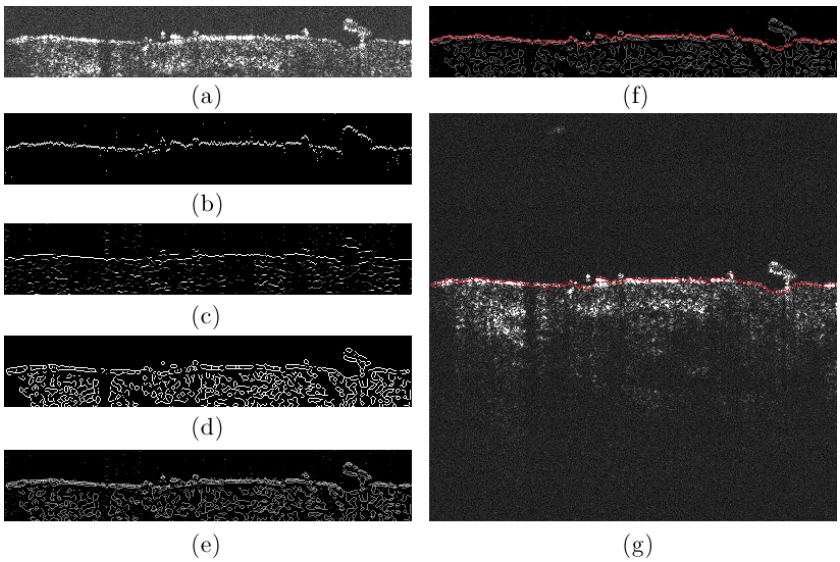


Fig. 2. Energy map step. (a) ROI of raw image. (b) intensity detector. (c) Sobel detector. (d) Canny detector (e) weighted energy map. (f) red line: shortest-path profile. (g) red line: extracted surface.

The cost of a path $P$ is defined as the sum of pixel value in the path added with the cost of roughness,[15]

$$C = \sum_{j=1}^{400} E(n_j, j) + \lambda_r \sum_{j=2}^{399} (n_{j-1} - 2n_j + n_{j+1})^2, \quad (3)$$

where $\lambda_r$ is the weighted factor. Using regularized shortest path extraction,[15] the contour of the skin surface is extracted, as shown in Figs. 2(f) and 2(g).

## 2.4. *ET measurement*

At first, a 9th-order polynomial fit is applied to smooth the extracted surface profile, as shown in green curve in Fig. 3(a). The averaged A-scan intensity is then defined as the intensity average of all the points in the green fitting curve. Subsequently at every depth the averaged A-scan intensity can be calculated, as shown in Fig. 3(b).

A threshold is needed to separate the dermis and epidermis area, which is defined as the average of 2nd maximum value and the lowest value between 1st and 2nd peak. From local minimum to 2nd maximum, the first position whose value exceeds the threshold is treated as junction between dermis and epidermis. ET is defined as the distance between air-skin surface and dermis-epidermis junction.

## 2.5. *Calculation of Intensity of Dermis*

In PWS OCT images, the appearance of capillary dilation and malformation are dark area of round or horizontal band. Direct measurement of depth and diameter of these dark area is difficult, due to the following reasons. Firstly, the intensity along the depth direction decays rapidly, conventional snake edge detection[16] could not obtain an enclosure contour. Secondly, region-based segmentation method also suffers from boundary leakage, due to the inevitable speckle noise[17] in OCT image. Complicated model[18] considering intensity, inhomogeneity and speckle noise is time consuming. Furthermore, shadowing artifacts or saturation artifacts may lead to false segmentation using these algorithms. Therefore, in this case, it is beneficial to use the average A-scan analysis once more to achieve the relative intensity of dermis, representing the vascular density. The averaged intensity of last 20 points is considered as the background intensity. Both averaged background intensity $I_{\text{bg}}$ and standard deviation $SV_{\text{bg}}$ are calculated to obtain the threshold, defined as $(I_{\text{bg}} + 7SV_{\text{bg}})$, to separate the dermis area and background area. If the averaged intensity of a depth position exceeds the threshold, this position is considered as the dermis lower boundary. To compare the dermis intensity of different OCT images with different noise level, we use relative intensity of dermis instead of absolute dermis intensity. The relative intensity of dermis is

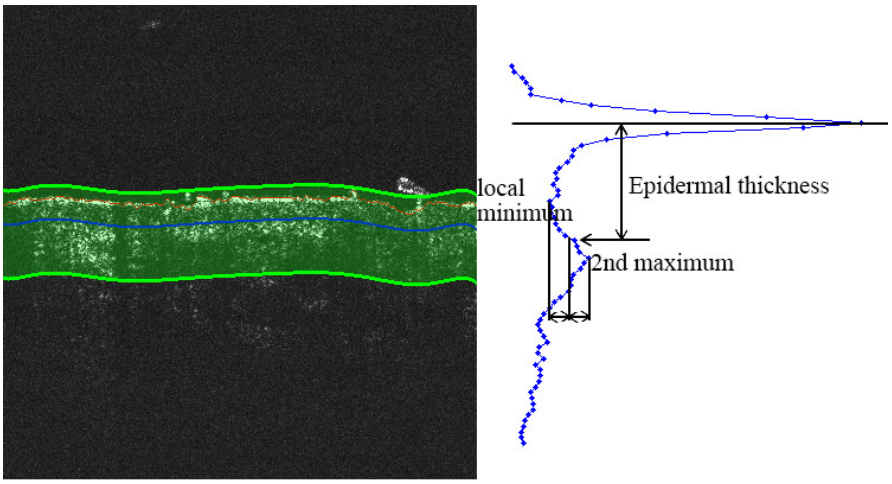


Fig. 3. ET measurement. (a) surface profile. red line: air-skin surface, green line: fitting curve, blue line: dermal-epidermal junction (b) average A-Scan analysis.

given by:

$$\mathrm{RID} = \alpha \cdot \frac{I_{\mathrm{dermis}}}{I_{\mathrm{bg}}}, \tag{4}$$

where RID, $I_{\mathrm{dermis}}$, $I_{\mathrm{bg}}$ and $\alpha$ are relative intensity of dermis, averaged intensity of dermis, averaged background intensity and scale factor, respectively. The parameter $\alpha$ is chosen to be 100.

## 3. Result and Discussion

A total of 83 automated measurements of ET are compared with manual line drawing method performed by experienced operator. The Pearson correlation coefficient $r$ is 0.947, as shown in Fig. 4. The agreement between automated and manual measurement is displayed in the Bland–Altman plot of Fig. 5. The mean thickness error between the proposed algorithm and the operator is $\sim 7.5\,\mu$m. Note that the axial resolution is $7.4\,\mu$m, the result proves that the automated measurement can replace the manual measurement with an accuracy equivalent to the spatial resolution of OCT image and is therefore good enough for clinical application. The precision of the algorithm can be improved through using sub-pixel detection or averaging several B-Scan ET.[19]

The method can be successfully applicable for OCT images that have saturation and shadowing artifacts, as shown in Fig. 6(b). Also, the algorithm shows good result on low-contrast OCT images, as shown in Fig. 6(d).

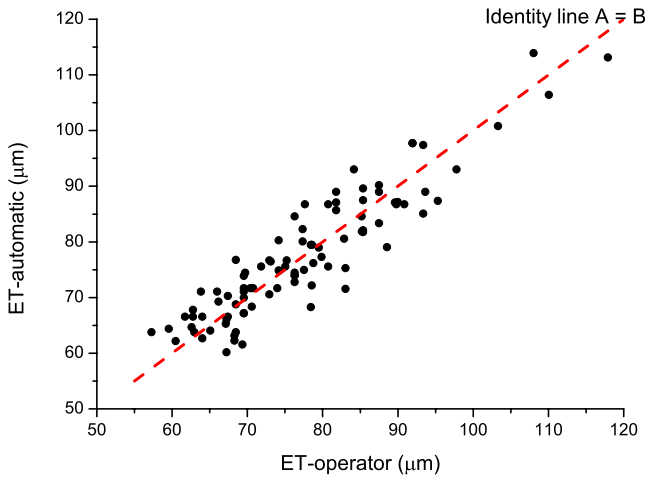


Fig. 4. Correlation between automated and manual measurement.

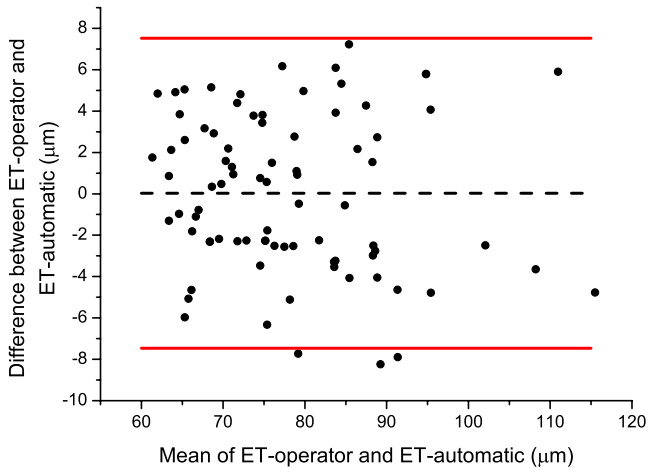


Fig. 5. Bland–Altman plot.

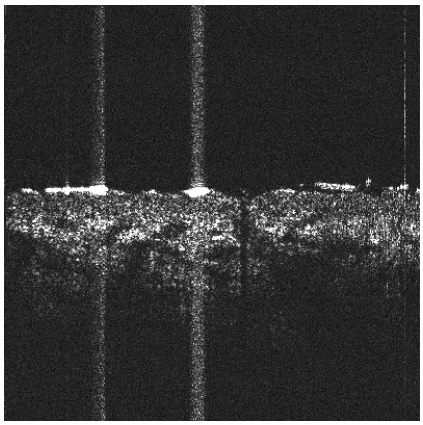

(a)

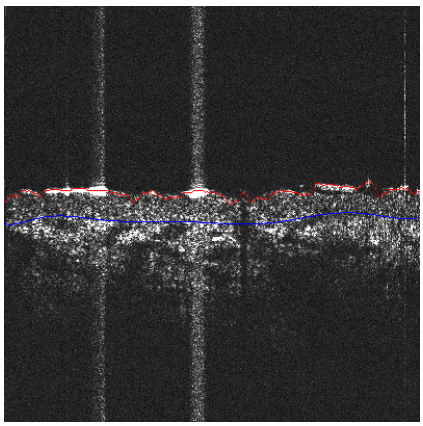

(b)

Fig. 6. (a) OCT image with saturation and shadowing artifacts. (b) ET measurement. Red line: air-skin surface. Blue line: dermal-epidermal junction (c) low-contrast OCT image. (d) Only skin surface can be detected.

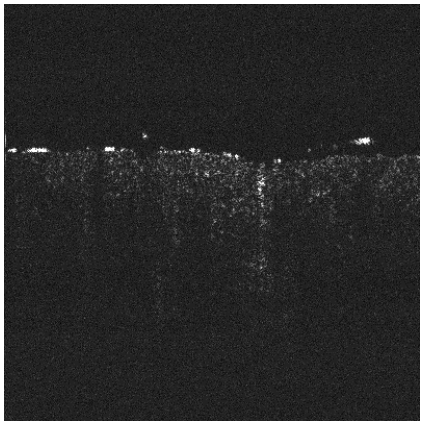

(c)

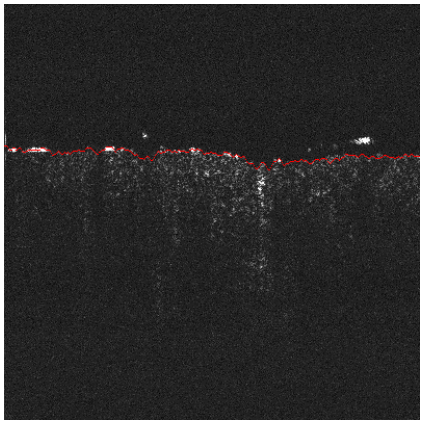

(d)

Fig. 6. (*Continued*)

The measured relative intensity of dermis in PWS skin and contralateral normal skin are $208.8 \pm 16.1$ and $253.1 \pm 21.8$, respectively, as shown in Table 1. There is a statistical difference between them ($p < 0.01$), because OCT image of PWS skin has low relative intensity due to capillary dilation.

ET is useful in diagnosis of different PWS skin type, especially in proliferative type whose skin surface is thickened.[10] In addition, ET is a good indicator of complication after PDT. The relative intensity of dermis reflects the vascular density in dermis, which is an important parameter in PDT mathematic model[20] and very useful for determining laser dose in PDT. Therefore, the automated measurements of ET and dermis relative intensity are operator independent and can provide an objective real-time assessment of PWS in clinic.

Table 1. Dermis relative intensity measurements of PWS skin and contralateral normal skin.

| | PWS skin | Contralateral normal skin |
|---|---|---|
| Dermis Relative Intensity | 208.8 ± 16.1 | 253.1 ± 21.8[a] |

[a]$p < 0.01$.

## 4. Conclusion

We implemented an automated algorithm to obtain ET and relative intensity of dermis from clinical OCT images. The automated measured ET is in good correlation and agreement with manual measurement. It is beneficial to use the automated method instead of manual measurement as an objective and accurate assessment of PWS. The relative intensity of dermis shows statistical difference between PWS skin and normal skin. This parameter is useful in simulating PDT mathematic model and determining laser dose in PDT. In the past, because of the lack of vascular structural information, PWS diagnosis and PDT treatments are generally conservative, and the dose of laser exposure is primarily based on the doctor's previous experience. Our work on automated assessment of epidermal thickness and vascular density of PWS OCT Image can provide quantitative assessment of PWS and PDT treatments and will be of high value in clinic.

## Acknowledgments

This work was supported in part by the National Natural Science Foundation of China under Grant 61227807, by the Ministry of Science and Technology of China under contracts 2006AA02Z472, 001CB510307 and 2009CB929400, by the Ministry of Education of China Grant 20130002110079 for Doctoral Program and by the Tsinghua Initiative Scientific Research Program Grant 2013THZ02-3.

## References

1. L. O. Svaasand, G. Aguilar, J. A. Viator, L. L. Randeberg, S. Kimel, J. S. Nelson, "Increase of dermal blood volume fraction reduces the threshold for laser-induced purpura: Implications for port wine stain laser treatment," *Lasers Surg. Med.* **34**(2), 182–188 (2004).

2. T. Gambichler, V. Jaedicke, S. Terras, "Optical coherence tomography in dermatology: Technical and clinical aspects," *Arch. Dermatol. Res.* **303**(7), 457–473 (2011).
3. Y. Hori, Y. Yasuno, S. Sakai, M. Matsumoto, T. Sugawara, V. Madjarova, M. Yamanari, S. Makita, T. Yasui, T. Araki, M. Itoh, T. Yatagai, "Automatic characterization and segmentation of human skin using three-dimensional optical coherence tomography," *Opt. Express* **14**(5), 1862–1877 (2006).
4. Z. Liu, Z. Guo, Z. Zhuang, J. Zhai, H. Xiong, C. Zeng, "Quantitative optical coherence tomography of skin lesions induced by different ultraviolet b sources," *Phys. Med. Biol.* **55**(20), 6175–6185 (2010).
5. Z. M. Liu, H. Q. Zhong, J. Zhai, C. X. Wang, H. L. Xiong, Z. Y. Guo, "Acute skin lesions following psoralen plus ultraviolet a radiation investigated by optical coherence tomography," *Laser Phys.* **23**(8), 085601 (2013).
6. S. Wu, H. Li, X. Zhang, Z. Li, "Optical features for chronological aging and photoaging skin by optical coherence tomography," *Lasers Med. Sci.* **28**(2), 445–450 (2013).
7. A. E. Karsten, "Effect of wavelength, epidermal thickness and skin type on the required dose for photodynamic therapy", in *Proc. Int. Conf. World Association of Laser Therapy*, pp. 137–143 (2008).
8. T. Wang, C. Wang, N. Huang, J. Zhang, Y. Gu, P. Xue, "Handheld optical coherence tomography device for photodynamic therapy," *Chinese Sci. Bull.* **57**(5), 450–454 (2012).
9. S. Zhao, Y. Gu, P. Xue, J. Guo, T. Shen, T. Wang, N. Huang, L. Zhang, H. Qiu, X. Yu, "Imaging port wine stains by fiber optical coherence tomography," *J. Biomed. Opt.* **15**(3), 036020–036020 (2010).
10. Y. Zhou, D. Yin, P. Xue, N. Huang, H. Qiu, Y. Wang, J. Zeng, Z. Ding, Y. Gu, "Imaging of skin microvessels with optical coherence tomography: Potential uses in port wine stains," *Exp. Ther. Med.* **4**(6), 1017 (2012).
11. J. Weissman, T. Hancewicz, P. Kaplan, "Optical coherence tomography of skin for measurement of epidermal thickness by shapelet-based image analysis," *Opt. Express* **12**(23), 5760–5769 (2004).
12. A. Krüger, T. Schwabe, M. Cuevas, P. Knuschke, E. Koch, "Measurement of the epidermal thickness with fourier domain optical coherence tomography in an occupational health study on natural sun protection of the human skin," in *Advances in Medical Engineering*, Vol. 114, pp. 349–354 (2007).
13. G. Josse, J. George, D. Black, "Automatic measurement of epidermal thickness from optical coherence tomography images using a new algorithm," *Skin Res. Technol.* **17**(3), 314–319 (2011).
14. H. Ding, J. Q. Lu, W. A. Wooden, P. J. Kragel, X.-H. Hu, "Refractive indices of human skin tissues at eight wavelengths and estimated dispersion relations between 300 and 1600 nm," *Phys. Med. Biol.* **51**(6), 1479 (2006).
15. M. Buckley, J. Yang, "Regularised shortest-path extraction," *Pattern Recogn. Lett.* **18**(7), 621–629 (1997).
16. M. Kass, A. Witkin, D. Terzopoulos, "Snakes: Active contour models," *Int. J. Comput. Vis.* **1**(4), 321–331 (1988).
17. J. M. Schmitt, S. H. Xiang, K. M. Yung, "Speckle in optical coherence tomography," *J. Biomed. Opt.* **4**(1), 95–105 (1999).
18. C. Li, R. Huang, Z. Ding, J. Gatenby, D. N. Metaxas, J. C. Gore, "A level set method for image segmentation in the presence of intensity inhomogeneities with application to mri," *IEEE Trans. Image Process.* **20**(7), 2007–2016 (2011).
19. F. Malmberg, J. Lindblad, I. Nystrom, Sub-pixel segmentation with the image foresting transform, in *Combinatorial Image Analysis*, P. Wiederhold, R. Barneva, Eds., Lecture Notes in Computer Science, Vol. 5852, pp. 201–211, Springer, Berlin Heidelberg (2009).
20. N. Huang, G. Cheng, X. Li, Y. Gu, F. Liu, Q. Zhong, Y. Wang, J. Zen, H. Qiu, H. Chen, "Influence of drug-light-interval on photodynamic therapy of port wine stains simulation and validation of mathematic models," *Photodiagnosis Photodyn. Ther.* **5**(2), 120–126 (2008).